Magnetic Resonance Imaging 77 (2021) 204–212

Contents lists available at ScienceDirect

Magnetic Resonance Imaging

journal homepage: www.elsevier.com/locate/mri

Original Contribution

Effects of motion correction, sampling rate and parametric modelling in dynamic contrast enhanced MRI of the temporomandibular joint in children affected with juvenile idiopathic arthritis

Lea Starck [a,b,*], Erling Andersen [b,c], Ondřej Macíček [d], Oskar Angenete [e,f], Thomas A. Augdal [g,h], Karen Rosendahl [h], Radovan Jiřík [d], Renate Grüner [a,b,i]

[a] Department of Physics and Technology, University of Bergen, Bergen, Norway
[b] Mohn Medical Imaging and Visualization Centre, Haukeland University Hospital, Bergen, Norway
[c] Department of Clinical Engineering, Haukeland University Hospital, Bergen, Norway
[d] Institute of Scientific Instruments of the Czech Academy of Sciences, Brno, Czechia
[e] Department of Radiology and Nuclear Medicine, St. Olav Hospital HF, Trondheim, Norway
[f] Department of Circulation and Medical Imaging, Norwegian University of Science and Technology, Trondheim, Norway
[g] Section for Paediatric Radiology, University Hospital of North Norway, Tromsø, Norway
[h] Department of Clinical Medicine, UiT The Arctic University of Norway, Norway
[i] Department of Radiology, Haukeland University Hospital, Bergen, Norway

ARTICLE INFO

Keywords:
JIA
TMJ
DCE MRI
Sampling rate
Motion correction

ABSTRACT

The temporomandibular joint (TMJ) is typically involved in 45–87% of children with Juvenile Idiopathic Arthritis (JIA). Accurate diagnosis of JIA is difficult as various clinical tests, including MRI, disagree. The purpose of this study is to optimize the methodological aspects of Dynamic Contrast Enhanced (DCE) MRI of the TMJ in children. In this cross-sectional study, including data from 73 JIA affected children, aged 6–15 years, effects of motion correction, sampling rate and parametric modelling on DCE-MRI data is investigated. Consensus among three radiologists determined the regions of interest. Quantitative perfusion parameters were estimated using four perfusion models; the Adiabatic Approximation to Tissue Homogeneity (AATH), Distributed Capillary Adiabatic Tissue Homogeneity (DCATH), Gamma Capillary Transit Time (GCTT) and Two Compartment Exchange (2CXM) models. Effects of motion correction were evaluated by a sum of least squares between corrected raw data and the GCTT model. The effect of systematically down sampling the raw data was tested. The sum of least squares was computed across all pharmacokinetic models. Relative difference perfusion parameters between the left and right TMJ were used for an unsupervised k-means based stratification of the data based on a principal component analysis, as well as for a supervised random forest classification. Diagnostic sensitivity and specificity were computed relative to structural image scorings. Paired sample *t*-tests, as well as ANOVA tests, were used (significant threshold: $p < 0.05$) with Tukeys post hoc test. High-level elastic motion correction provides the best least square fit to the GCTT model (percental improvement: 72–84%). A 4 s sampling rate captures more of the potentially disease relevant signal variations. The various parametric models all leave comparable residues (relative standard deviation: 3.4%). In further evaluation of DCE-MRI as a potential diagnostic tool for JIA a high-level elastic motion correction scheme should be adopted, with a sampling rate of at least 4 s. Results suggest that DCE-MRI data can be a valuable part in JIA diagnostics in the TMJ.

1. Introduction

Juvenile Idiopathic Arthritis (JIA) encompasses all cases of arthritis of unknown origin with onset prior to the 16th birthday, persisting for a minimum of 6 weeks [1]. Reported JIA prevalence varies between 0.07 and 4.01 per 1000 children [2]. Continuation of active disease into

* Corresponding author at: Allégaten 55, 5007 Bergen, Norway
E-mail addresses: lea.starck@uib.no (L. Starck), erling.andersen@helse-bergen.no (E. Andersen), macicek@isibrno.cz (O. Macíček), Oskar.Angenete@stolav.no (O. Angenete), Thomas.Angell.Augdal@unn.no (T.A. Augdal), Karen.Rosendahl@unn.no (K. Rosendahl), jirik@isibrno.cz (R. Jiřík), eli.renate.gruner@helse-bergen.no (R. Grüner).

https://doi.org/10.1016/j.mri.2020.12.014
Received 3 September 2020; Received in revised form 7 December 2020; Accepted 20 December 2020
Available online 13 January 2021

adulthood has, depending on the study, been reported for 41% and 67% of the patient cohort [3,4]. Early effective treatment is contingent on early detection of the disease, yet therapeutic interventions are often hampered by differing methodologies and asymptomatic temporomandibular joints (TMJs) [2,5,6]. Inflammation in the (TMJ) are frequently reported in cases of JIA, and it is estimated that the TMJ may be involved in between 45% and 87% of the cases [5], [7–10].

Methods for detecting JIA-involvement of the TMJ include structural imaging (radiographs, ultrasound, computed tomography and MRI) and clinical assessment including restricted mouth opening, mandibular deviation during mouth opening, facial asymmetry, and history of pain. [5], [10–13]. Reading of structural MRI images post contrast injection (i.e. T1 static) is currently one of the most sensitive assessment methods [8,9], [11]. Even though a variety of MRI techniques for examination of the temporomandibular joint exist, static images remain the gold standard. The TMJ may also be studied under the hypothesis that the inflammation is an origin of pain, accompanied by increased vascularity [8,14,15]. In addition to the MRI techniques recently reviewed [16], the TMJ may also be assessed with Dynamic Contrast Enhanced (DCE)-MRI. To capture the increased vascularity, the microvasculature may be assessed by measuring the change in signal intensity due to the passing of a contrast agent in time (i.e. T1 dynamic) [8]. DCE-MRI dynamics can be studied by means of semi-quantitative measures derived directly from the signal intensity time curves [17–19] or by tracer kinetic modelling [20,21]. No standard pipeline to process the DCE-MRI data in the temporomandibular joint exists. There are several models that can be applied in tracer kinetic modelling. A general feature of these approaches is that the capillary bed is regarded as a box (being the imaged tissue voxel or region of interest) with an inlet and an outlet, where blood containing contrast agent flows in and out, respectively. The contrast agent may also diffuse back and forth across the capillary wall. It is assumed that the system is linear and time invariant, and that contrast agent is neither generated nor destroyed in the system [21,22]. In general, the change in the measured contrast agent concentration within the capillary bed, $C(t)$, is the sum of all in-fluxes with the sum of all out-fluxes subtracted, Eq. (1),

$$\frac{dC(t)}{dt} = \sum_{in} J_i(t) - \sum_{out} J_o(t) \tag{1}$$

where $J_i(t)$ is the in-flux and $J_o(t)$ is the out-flux [21]. The concentration at the input of the voxel is called an arterial input function (AIF). The measured tracer concentration, $C(t)$, is determined by the impulse response of the system and is given by the convolution in Eq. (2),

$$C(t) = \int_0^t C_p(\tau)\cdot i(t-\tau)dt = [x * i](t) \tag{2}$$

where $C_p(t)$ is the AIF and $i(t)$ is the impulse response [21]. The impulse response is given by the specific model describing the microvasculature. Each model has several analytical parameters that are varied to provide the best fit between the left- and right-hand side of Eq. (2).

The aim of the current study is to explore the feasibility of DCE-MRI in the diagnosis of TMJ involvement in JIA. Methodological aspects of motion correction, signal sampling and parametric modelling are evaluated. Three levels of motion correction were applied and the results on the data examined and the sampling rate capturing the dynamics of the TMJ is investigated, [23]. Additionally, the ability of the Adiabatic Approximation to the Tissue Homogeneity Model (AATH), Distributed Capillary Adiabatic Tissue Homogeneity Model (DCATH), Gamma Capillary Transit Time Model (GCTT) and Two Compartment Exchange Model (2CXM) to produce parameters that are able to distinguish between presumed healthy and affected TMJ are examined. Finally, it is discussed if DCE-MRI can be of added value in the diagnosis of JIA affected TMJ.

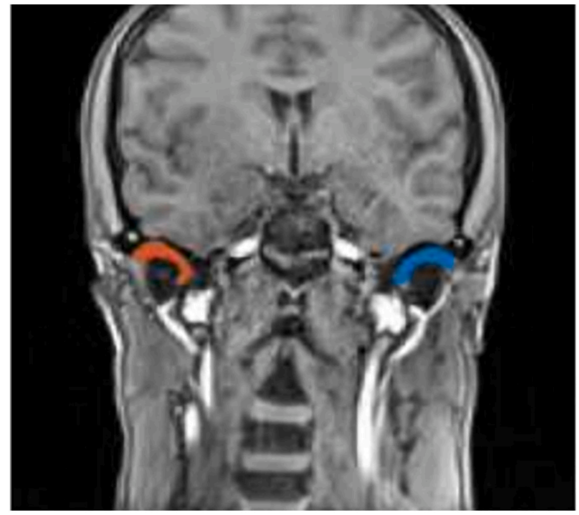

Fig. 1. Regions of interest, covering left (blue) and right (red) TMJ. (For interpretation of the references to colour in this figure legend, the reader is referred to the web version of this article.)

2. Material and methods

2.1. Data collection

All data were acquired and used in agreement with ethical approval from REK Vest. Written informed consent was obtained from their care takers and participants older than 12 years. DCE-MRI was included as part of an extensive, longitudinal, multicentre study on quality of life, oral health and imaging in JIA (the Norwegian study in JIA, Nor JIA), in a larger group of children. The analysed data consists of DCE-MRI acquisitions of the TMJ in a subset of 73 children, aged 6–15 years, diagnosed with JIA with possible TMJ involvement. The data constitutes a balanced subset of patients ranging from radiologically severe arthritis to cases with only subtle findings. With a sampling rate of 4 s, 60 image volumes (160x160x16 image matrices) were acquired from each participant, using a MAGNETOM Skyra 3 T system (Siemens Healthineers, Erlangen, Germany), using a 64-channel head coil and a 3D-FLASH sequence (TR/TE/FA = 4 ms/1 ms/9°). The contrast agent Gd-DOTA i.e. Dotarem®, (Guerbet, Villepinte, France) was injected at a rate of 5 mL/s, at 10 s after acquisition start, using a power injector and a subsequent saline injection. The MRI data was collected at three study sites, using identical acquisition parameters. Clinical scores derived from assessment of structural MR images determined a measurement of likelihood of affected and unaffected TMJs. The assessment was performed by a by an expert paediatric radiologist. These scores were available from the local site only, comprising 52 participants. Among these 11 participants were deemed to have affected TMJ, 41 participants to have unaffected TMJ.

2.2. Data processing

Regions of interest were defined by manually selected masks, covering the left and right synovial TMJ, respectively, in the 5th imaged volume (acquired 20 s after acquisition start), Fig. 1. These were based on a consensus among three radiologists with between 5 and 15 years of experience. The DCE-MRI was acquired in coronal plane but several other acquisitions in both sagittal and coronal plane were also available to the image readers. When drawing the ROIs (on the coronal DCE-acquisition) the involved image readers (trained radiologists) carefully checked the location of the ROI also in sagittal plane, thereby avoiding the retrodiscal area and areas of abundant joint fluid. It is probably not possible to fully separate condylar cartilage from synovium. However,

Table 1
Parameter descriptions. Semi-quantitative (*RT, M, S, A*) and quantitative (F_p, *E*, *ve*, T_c, α^{-1}, σ, *BAT* and *PS*) perfusion parameters, estimated by application of the pharmacokinetic models.

Parameter	Unit	Description
RT	s	Time from baseline to the first maximum of relative enhancement curve
M	–	First maximum value of the relative enhancement curve
S	–	Slope of the relative enhancement curve tail
A	–	Area under the relative enhancement curve
F_p	ml/ml/min	Blood plasma flow
E	–	Extraction fraction
ve	–	Extravascular extracellular fraction
T_c	min	Mean capillary transit time
α^{-1}	–	Width of the capillary transit time distribution
σ	min	Standard deviation of mean transit time
BAT	min	Bolus arrival time (AIF vs ROI delay)
PS	ml/ml min	Permeability surface product

contrast enhancement of the condylar cartilage is not a known marker of active inflammation in TMJ and does therefore not pose a diagnostic problem in this setting.

Relative enhancement curves were extracted from the DCE-MRI data by averaging pixel signal values contained in the regions of interest, subtracted and divided by the baseline signal, (signal - baseline)/baseline. Semi-quantitative perfusion parameters, Table 1 were computed directly from the relative enhancement curves.

Quantitative perfusion parameters, Table 1, were estimated using an inhouse developed MATLAB tool, version R2017a, (MathWorks Inc., Natick, Massachusetts, US). An AIF was not measured for each individual TMJ. Instead, a population-based AIF based on a random sample of 22 participants was used in the analysis. The 22 individual AIFs were selected semi-automatically by choosing voxels with the highest signal peak within a region containing the large brain feeding arteries. By finding delay between peaks, the AIFs were temporally aligned, and a median AIF calculated. The median AIF is composed of two peaks (due to the first and second bolus passage). The final AIF was obtained by a parametric fit and scaling according to the Parker model [24,25].

According to a previous study [26], it is unlikely that both TMJs in one participant are equally affected. In the following, relative parameter difference between the left and right TMJ, Eq. (3), are reported,

$$P_{rel} = \frac{|P_{left} - P_{right}|}{P_{left} + P_{right}} \tag{3}$$

where P_{left} and P_{right} are the parameters derived from the left and right TMJ, respectively and P_{rel} is the ensuing relative parameter difference. Since relative parameter differences between the left and right TMJ are reported the choice of using an identical AIF, in this case a population-based AIF, is motivated by the goal of highlighting the asymmetry between the joints.

2.3. Pharmacokinetic models

The Adiabatic Approximation to the Tissue Homogeneity Model (AATH) assumes a plug-flow of the blood through the intravascular space, so that the tracer concentration, $c(x,t)$ is dependent on the distance x from the inlet and the time t after the tracer enters at the inlet. The extravascular extracellular space (EES) is modelled as a single compartment [22], [27–29], and the contrast agent is assumed to cross the capillary wall only at the outlet (adiabatic approximation). Exchange of the contrast agent between the intra- and extra-vascular space is assumed in both directions.

Since there is both many capillaries and EES inside a DCE-MRI voxel, there will be a variation in transit times inside of each voxel. This is taken into account by the Distributed Capillary Adiabatic Tissue Homogeneity Model (DCATH), which measures the contrast agent concentration in a voxel as a sum of concentrations in the capillaries in the voxel, iteratively applying either a normal, truncated normal or skewed Gaussian distribution of transit times (in this study the truncated normal distribution was applied). DCATH model thus outputs an additional parameter σ, which is the standard deviation in transit times in a voxel [30].

The Gamma Capillary Transit Time Model (GCTT) also, like the DCATH model, takes into account that a DCE-MRI voxel contains many capillaries of different sizes, causing varying transit times of the contrast agent through the capillaries. However, the GCTT model assumes a gamma distribution of transit times [20]. It can be shown that other tracer kinetic models, such as the Tofts, Extended Tofts, the Two Compartment Exchange Model (2CXM) and the AATH model, are special cases of the GCTT model when different transit time distributions are applied [20]. A special parameter for the GCTT model is α^{-1}, which measures the width of the transit time distribution. α^{-1} varies between 0 and 1, representing the limiting cases of a delta function distribution ($\alpha^{-1} = 0$), corresponding to the AATH model and the exponential function distribution ($\alpha^{-1} = 0$), corresponding to the 2CXM model [20].

2.4. Effects of motion correction

In motion correction, an input image is adjusted to fit a reference image. Three levels of motion correction were applied successively; no image registration, primary (affine) registration and elastic registration. A common parametric approach is to define a transformation which will align an input $\boldsymbol{x}$ image to the reference image, Eq. (4),

$$\boldsymbol{T}(\boldsymbol{x}) = \boldsymbol{A}\boldsymbol{x} + \boldsymbol{t} \tag{4}$$

where $\boldsymbol{T}(\boldsymbol{x})$ is the transformation function, $\boldsymbol{A}$ is a matrix containing parameters, that in the case of affine registration allow rotation, scaling and skewing of the input image. The vector $\boldsymbol{t}$ contains parameters causing translation of the input image. The open source software Elastix [31,32] was used to implement a 3D affine registration. Thus, by finding the optimal four times three parameters of $\boldsymbol{A}$ and $\boldsymbol{t}$, the 3D affine registration should correct for translational or rotational movements of the region of interest (head). The time series volumes were aligned to volume number five, which was acquired 20s after acquisition start. At this time the contrast agent was injected, but not accumulated in the region of interest. This volume was also used to draw the regions of interest, Fig. 1. Initial transformation parameters, as well as other details of the affine registration as applied with the Elastix software [31–33], are defined in a publicly available parameter text file [34].

The time series volumes were expected to exhibit varying levels of contrast, due to changes in tracer concentration in time. Therefore, mutual information [35] was chosen as an alignment quality measure on which to base the cost function of the motion correction transformation. Due to differences in tracer levels, a pixel in the reference image may have an intensity value that differs from the intensity value in the corresponding pixel in the input image. A two-dimensional histogram plot comparing the intensity values of input (x-axis) and reference image (y-axis), respectively, governs the approach. Lower degree of entropy in the histogram plot expresses more accurate image registration [35]. The transformation parameters were optimized using an iterative process dubbed adaptive stochastic gradient descent [31,36].

A second motion correction algorithm was applied on the affine registered images. This was an elastic motion correction scheme, originally developed in-house for registration of kidney images [37]. In the elastic motion correction scheme, the regions of interest (i.e. the gross TMJ volumes) were co-registered to later time points independent from the rest of the image. After registration of the regions of interest, they are re-inserted into the image. The registration is based on co-aligned image intensity gradient vectors in the input and reference image. However, image intensities vary in time due to the passing of contrast agent.

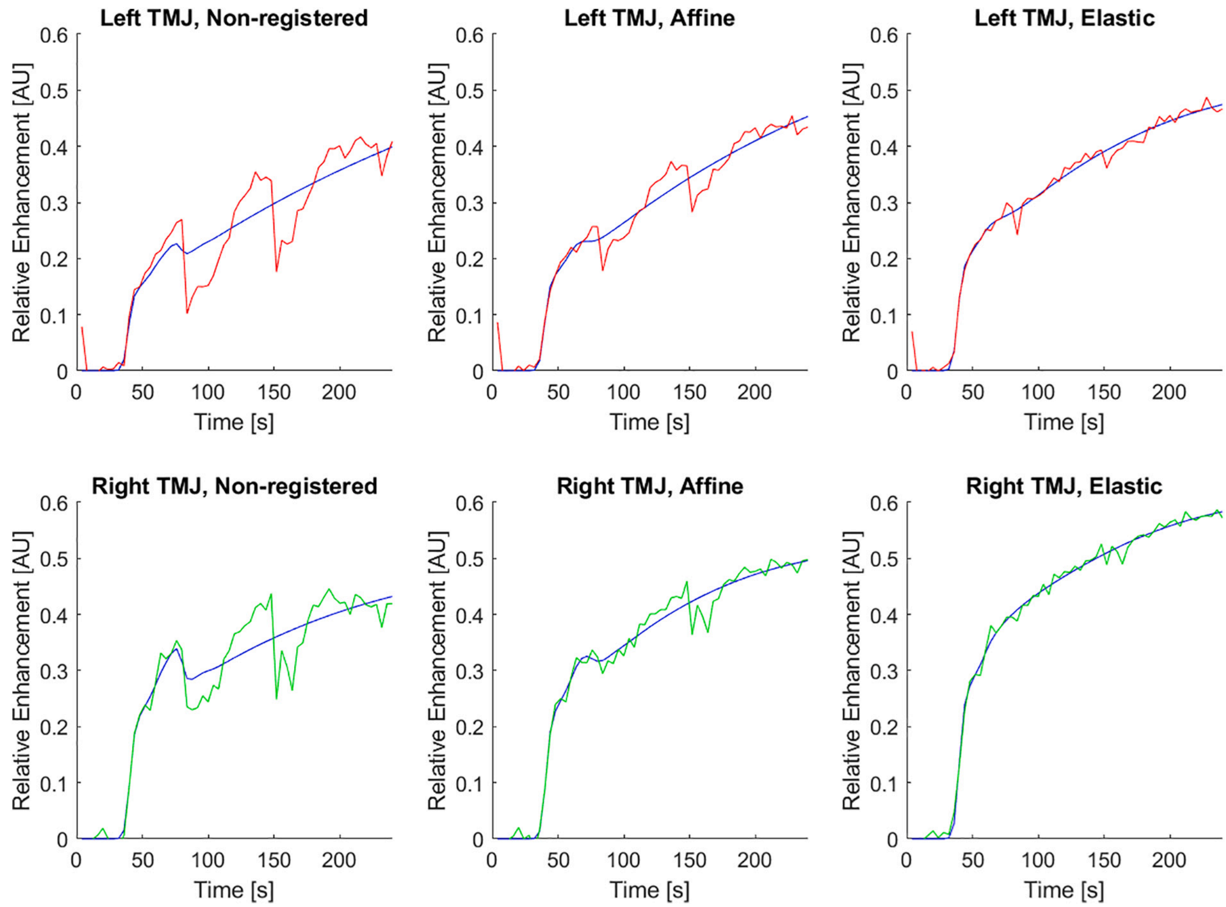

Fig. 2. Effects of three levels of motion correction in a random participant. Relative contrast agent enhancement curves from the left Temporomandibular Joint (TMJ) (upper row, red), right TMJ (lower row, green). DCE-MRI signal with no motion correction (left column), signal after affine motion correction (middle column) and signal after elastic registration (right column). The pharmacokinetic model GCTT is overlaid (blue). (For interpretation of the references to colour in this figure legend, the reader is referred to the web version of this article.)

Therefore, the gradients in the input and reference image are normalized. [37]. Normalizing the gradients meant removing their amplitude, letting the gradient vector entries take on relative values between 0 and 1, while the gradient direction remains the same, such that the geometrical outlines in the region of interest could be exploited.

2.5. Effects of sampling rate

The imaging data was acquired with a 4 s sample rate. Decreased sampling rates were mimicked by re-binning and averaging signal samples into bins of size 2, 3, 4 and 5. The results are relative enhancement curves with temporal resolutions of 8 s, 12 s, 16 s and 20 s, respectively. To investigate the effect of sampling rate on the information in the sampled signal, semi-quantitative relative parameter differences (P_{rel}) were computed and compared across the temporal resolutions.

2.6. Data-driven stratification of participants

Four semi-quantitative parameters and seven quantitative parameter differences were defined, Table 1. Each of the parameters was standardized and principal component analysis performed with Scikit-learn [38].

Using the MATLAB R2017a, (MathWorks Inc., Natick, Massachusetts, US) k-means clustering algorithm, the participants were divided into two groups based on four principal independent components, iteratively minimizing the distance between the vectors and the central point in each group. The k-means algorithm has a random starting point, and the results would therefore vary slightly in each run. To generate a basis for investigating the likelihood of a participant belonging to the group he or she would be assigned to the algorithm was implemented 1000 times. Finally, each participant was assigned a decimal number between -1 and $+1$, depending on the number of times the k-means algorithm would assign the participant to either of the groups. A positive number denoted the affected group, negative numbers denoted the unaffected group. A number close to $|-1|$ would indicate a greater probability for the participant belonging to his or her assigned group. A number closer to zero should not be interpreted as evidence that the corresponding individual is necessarily closer to the opposite group.

Data labels, i.e. structural image scorings, were available from the local cite, comprising 52 participants. These data were divided in balanced training and test sets and fitted to the random forest machine learning algorithm in Scikit-learn [38]. 75% (parameters from 39 participants) were used for training and 25% (parameters from 13 participants) were used for testing.

2.7. Statistics

The three levels of motion correction were compared by applying a least square fit (χ^2) between the measured data and the applied pharmacokinetic model (GCTT). Later analysis showed that the model curves do provide similar fits to the raw data. Moreover, since the GCTT model has an extra parameter, it would be more likely to overfit the data, and thus minimize the least square fit, making this a conservative approach. Three successive levels of motion correction (non-registered, affine and elastic) were compared based on a one-way ANOVA test. Tukey's post

Table 2
Sum of squares, χ^2, between the relative enhancement curves and the fitted GCTT model after different applied motion corrections (non-registered, affine and elastic) across 47 participants. Percentages in round brackets refer to the percental improvement relative to non-registered data.

Registration Method	Left TMJ	Right TMJ
	Sum of Squares	Sum of Squares
Not registered ($n = 47$)	2.18	3.74
Affine (n = 47)	0.95 (56%)	0.90 (76%)
Elastic (n = 47)	0.60 (72%)	0.60 (84%)

Table 3
Effects of motion correction on DCE-MRI relative parameter differences. Means, standard deviations and *p*-values comparing the relative parameter difference, P_{rel}, distributions (Blood plasma flow *Fp*, Extraction fraction *E*, EES volume *ve*, Capillary transit time T_c, GCTT transit time distribution width α^{-1} and Bolus arrival time *BAT*) obtained with different motion correction methods (Non-registration, Affine and Elastic) in the 47 participants in which it was possible to estimate GCTT parameters without prior motion correction. The p-values are computed using the ANOVA test with three independent variables; no motion correction, affine motion correction and elastic Significance threshold $p < 0.05$.

Parameter (unit)	No motion correction		Affine motion correction		Elastic motion correction		p-value
	Mean	Std. dev.	Mean	Std. dev	Mean	Std. dev.	
F_p	0.16	0.1	0.17	0.1	0.14	0.1	0.56
E	0.18	0.2	0.22	0.2	0.24	0.2	0.47
ve	0.62	0.4	0.62	0.4	0.61	0.4	0.98
T_c	0.28	0.3	0.27	0.2	0.23	0.2	0.51
α^{-1}	0.61	0.3	0.51	0.4	0.56	0.3	0.40
BAT	0.05	0.1	0.03	0.02	0.02	0.2	0.31

hoc test was applied to check for pairwise statistically differing means. The semi-quantitative parameter distributions of the GCTT model were visualized in boxplots with decreasing temporal resolutions, and with the different levels of motion correction applied. Semi-quantitative relative parameter difference (P_{rel}) distributions with low temporal resolutions (8 s, 12 s, 16 s and 20 s) were compared to the high temporal resolution (4 s) parameter distribution, using a paired sample *t*-test. *p*-values describing the levels of significance between the k-means clustered groups were computed based on a two-way ANOVA test with Tukeys post hoc test.

A significance threshold of $p = 0.05$ was selected in all statistical tests described above, meaning that any p-value lower than 0.05 indicates that the compared parameter distributions are statistically distinguishable.

3. Results

3.1. Effects of motion correction

Motion corrected relative enhancement curves from a randomly selected participant were overlaid by the GCTT model curves, Fig. 2, suggesting that elastic registration outperforms non-registration and affine registration. Without motion correction, the GCTT model failed to estimate parameters in 26 participants. The elastic registration scheme outperforms the affine registration, Table 2. The GCTT model was applied to the left and right TMJ from the remaining 47 participants. Measuring the sum-of-squares, χ^2, between the measured motion corrected data in each TMJ and the corresponding modelled curve for each level of motion correction (no motion correction, affine registration and elastic registration), a better fit to higher-level motion corrected data is observed, Table 3.

Estimated GCTT relative perfusion parameter differences (P_{rel}) do not display mean values that differ significantly, Fig. 3, nor are the

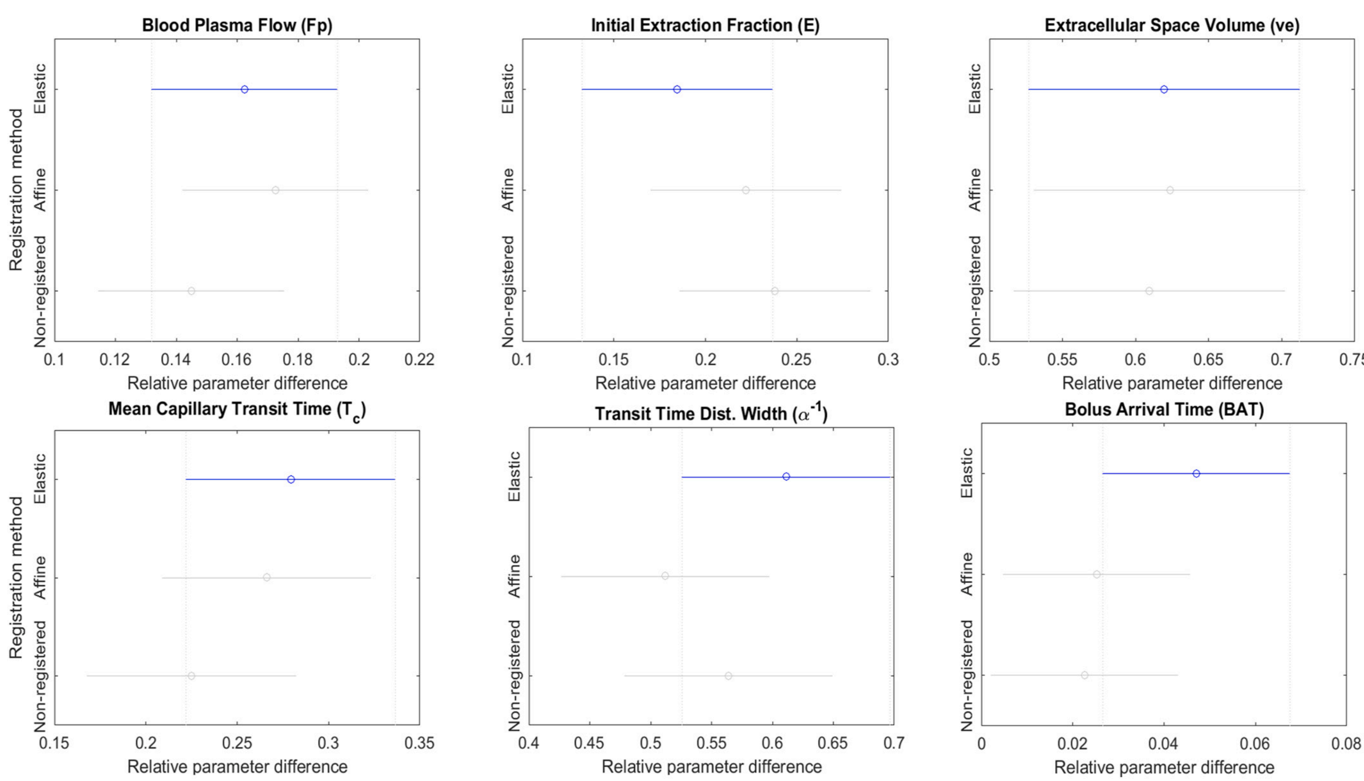

Fig. 3. Comparison of mean parameter values, P_{rel}, (Blood plasma flow *Fp*, Extraction fraction *E*, EES volume *ve*, Capillary transit time T_c, GCTT transit time distribution width α^{-1} and Bolus arrival time *BAT*) between the left and right TMJ obtained with different motion correction methods (Non-registration, Affine and Elastic) in 47 participants.

Table 4
Effects of sampling rate in DCE-MRI. Statistical differences in relative parameter difference distributions in the Temporomandibular Joint in 73 participants across sampling rates and degree of motion correction. Significance threshold $p < 0.05$.

Parameter	Registration scheme	8 s	12 s	16 s	20 s
Rise Time, *RT*	Not registered	**0.01**	< **0.005**	< **0.005**	< **0.005**
	Affine	**0.01**	< **0.005**	< **0.005**	< **0.005**
	Elastic	< **0.005**	< **0.005**	< **0.005**	< **0.005**
Max, *M*	Not registered	0.90	0.42	< **0.005**	< **0.005**
	Affine	0.72	0.97	< **0.005**	< **0.005**
	Elastic	**0.03**	**0.01**	< **0.005**	< **0.05**
Slope, *S*	Not registered	0.83	0.48	0.26	0.24
	Affine	**0.03**	0.23	0.06	< **0.005**
	Elastic	**0.01**	**0.01**	**0.04**	0.05
Area, *A*	Not registered	0.62	0.70	< **0.005**	< **0.005**
	Affine	0.48	0.29	< **0.005**	< **0.005**
	Elastic	**0.02**	0.07	< **0.005**	< **0.005**

The significance threshold was set to p=0.05, and hence all values in table 4 below this threshold were rendered in bold. Bold font was chosen for easy reading of the table, drawing the attention to the pattern of the data.

ANOVA *p*-values comparing the various motion corrected schemes significant, Table 3. Means, standard deviations and p-values comparing the relative parameter difference, P_{rel}, distributions obtained with different motion correction methods (Non-registration, Affine and Elastic) in the 47 participants in which it was possible to estimate GCTT parameters without prior motion correction were calculated, Table 4. With increasing the level of motion correction, the p-values comparing the semi-quantitative relative parameter differences (P_{rel}) in the lower resolution data to the high (4 s) resolution data tend to decrease but are not statistically significant.

3.2. Effects of sampling rate

Reducing sampling rate reduces the variability in the estimated semi-quantitative relative parameter differences, P_{rel}, Fig. 4. When successively comparing P_{rel} of high temporal resolution (4 s), with lower temporal resolution (8 s, 12 s, 16 s and 20 s), Table 4, the distributions P_{rel} also change significantly with sufficiently decreased sample rates. With elastic motion correction this happens when the temporal resolution drops from 4 s to 8 s and suggests that it is important to have a sampling rate of 4 s.

3.3. Data-driven stratification of participants

The four pharmacokinetic models are all suited to fit the DCE-MRI data, and differ little in performance, Fig. 5. The relative standard-deviation of the sum of squares of residuals between the elastic registered raw data curve and the model curves is 3.4%.

A k-means algorithm was applied to categorize the participants into two groups, group A and group B. This was to investigate if the models categorize the participants very differently, based on the relative parameter differences. Based on a comparison to structural image scorings, group A was assumed to correspond to unaffected individuals, and group B was assumed to correspond to affected participants. Out of the 73 participants, 62 individuals were placed in group A, and 11 individuals were placed in group B, when analysing the data with the GCTT model. Using the DCATH model instead, 59 individuals were placed in group A, and 14 were placed in group B. With the AATH model 66 individuals were placed in group A, and 7 individuals were placed in group B. Finally, with the 2CXM model, 63 individuals were placed in group A and 10 individuals were placed in group B.

Scorings, giving an indication of whether or not a participant was affected by JIA, based on structural MRI images were available for 52 of the 73 participants. Sensitivities and specificities were calculated assuming structural MRI data as the ground truth, using both unsupervised k-means stratification on all of the labelled data, as well as random forest classification on the balanced 25% of data used for testing of the random forest stratification, Table 5.

Across the pharmacokinetic models there was agreement about 52 participants; 51 of which were placed in group A, and one of which was placed in group B. Structural image scorings were available for 40 of the 52 participants between which there was agreement about group assignments across all pharmacokinetic models. Sensitivity of scores across models relative to the structural image scores was found to be 0, and the specificity 0.96. There clearly is an overlap between relative parameter differences *(P_{rel})* in affected and unaffected participants Fig. 6, where the parameters are calculated with the DCATH model and there is agreement between the k-means clustered groupings and the structural image scores in 41 cases. Based on a two-way ANOVA test (significance threshold <0.05) with the standardized relative parameters and group scorings as independent variables and Tukey's post hoc test, that neither the parameters, nor the interaction of parameters with group scorings were significant. However, group scorings were found to be significant ($p = 1.0 \cdot 10^{-6}$).

4. Discussion

There is need for more accurate diagnostic tests for JIA in general, since reported disease prevalence varies between 0.07 and 4.01 per 1000 children [2]. More specifically, reported TMJ involvement in confirmed cases of JIA covers a range from 45% to 87%, and this is largely due to differing diagnostic methodology and asymptomatic TMJ [2], [5–13]. In the current study DCE-MRI is explored as a potential tool to aid in the diagnosis.

We have examined the methodology in application of DCE-MRI as a possible diagnostic tool and found that a better fit to the GCTT model is obtained with high-level elastic motion correction. We recommend a sampling rate of at least 4 s to capture potentially disease relevant signal variations after application of high-level motion correction. The various parametric models all leave comparable and small residues. Since none of the applied perfusion models left a substantial residue and since they display comparable sensitivities and specificities relative to the structural image scores, in principle, all the models are potentially applicable to the TMJ. It remains to be tested whether one of the models outperforms the others in the diagnostics of JIA affected TMJ, and since the diagnostic criteria are still hampered by differing diagnostic methodologies, the model estimations must be evaluated in the light of more clinical data.

High-level motion correction, specifically elastic image registration, provides smoother relative enhancement curves and a better fit to the GCTT model approximation. The model approximation also becomes smoother with increasing levels of motion correction of the raw data. The statistical comparison between mean values of parameter distributions does not suggest that the post registration parameter distributions differ significantly from pre-registration parameter distributions. A large proportion of data stemming from minimally moving participants could be a reason for this. Even though estimated parameter values do not change on a population level, individual parameters might still be estimated more accurately when motion correction is applied.

Even without application of motion correction, the results of this study indicate that if the sampling rate is lower than 4 s, it is possible that important information about the dynamics in the TMJ is lost. The

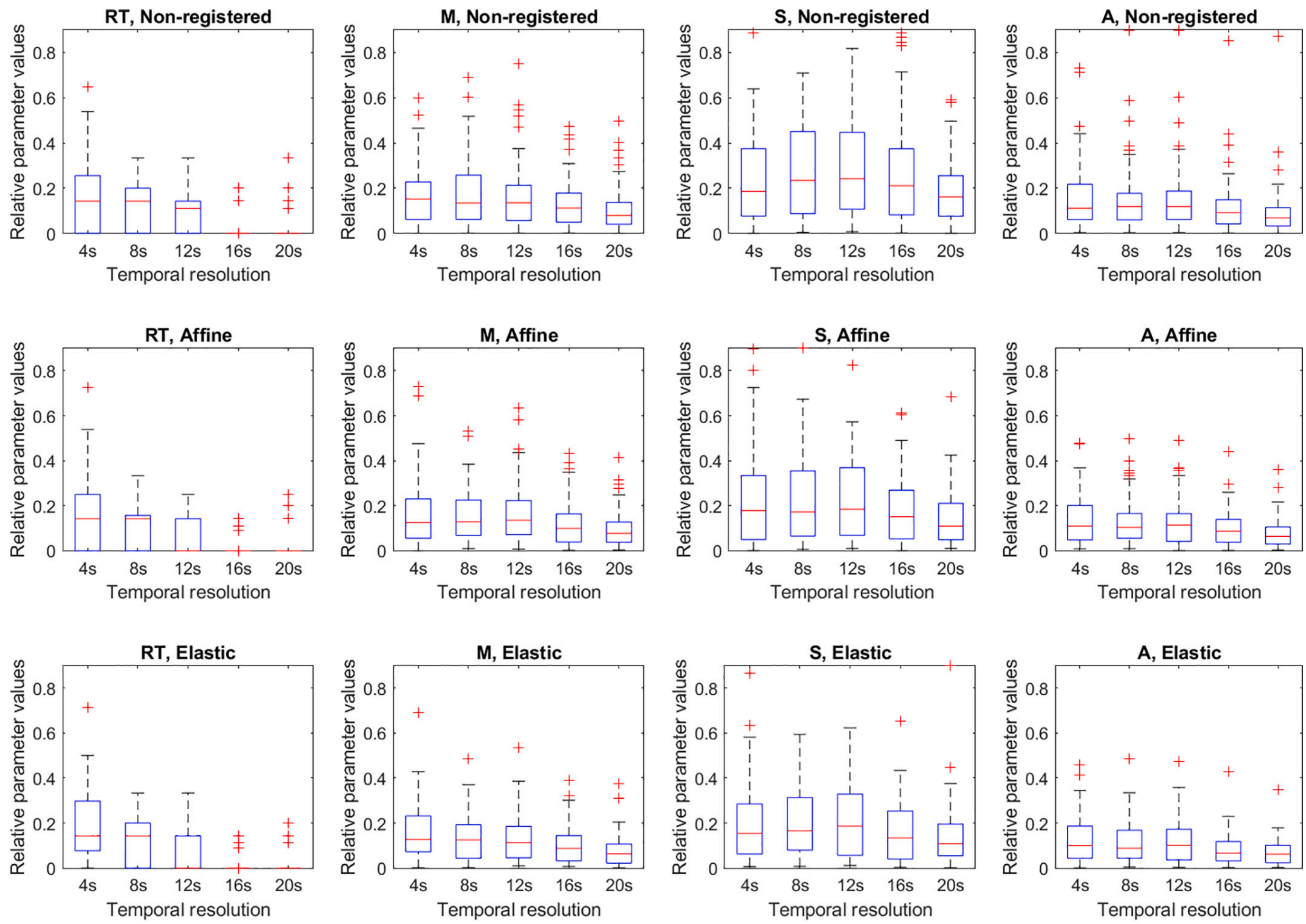

Fig. 4. Effects of sampling rates in DCE-MRI. Distributions of relative differences, P_{rel}, in semi-quantitative parameters (Rise time - *RT*, First maximum value - *M*, Slope of curve tail -*S* and Area under curve - *A*) between the left and right temporomandibular joints with decreasing temporal resolution after motion correction (top; non-registration, middle; affine registration, bottom; elastic registration) in 73 participants.

parameter distributions with diminishing temporal resolution become more dissimilar with a higher level of motion correction. This could also suggest the importance of high sampling rates to avoid loss of potentially valuable diagnostic information.

There is substantial overlap within detectable differences in parameter estimations between the left and right TMJ in presumed affected versus unaffected participants. However, DCE-MRI may be a feasible diagnostic tool in the evaluation of JIA affected TMJ, as a specific, rather than a sensitive tool. The current study focuses on the methodological aspects of DCE-MRI data processing, to ensure that the data can be evaluated in JIA diagnostics. Since no consensus yet exists in the evaluation of JIA affected TMJ, to further assess DCE-MRI data for this application, DCE-MRI data should be compared to other clinical data in a larger study cohort.

A limitation of this study is the use of a population-based AIF, as opposed to patient specific AIFs, since patient specific AIFs might be better suited for the description of individual biology. However, measuring individual AIFs would be user dependent, adding another level of variability to the data. A recent study did not find that patient specific AIFs improved the repeatability in the head and neck area [39]. Furthermore, we have been comparing relative perfusion parameter differences between the left and right TMJ. We have therefore assumed that inaccuracies that are not disease relevant, caused by the AIF are cancelled out. While it is unlikely that both TMJs are equally affected [26], one should keep in mind that the possibility that they are, though small, is still present. Our approach is conservative, in that if both TMJs should indeed be equally affected it would not contribute towards a positive conclusion about the DCE-MRI feasibility as a diagnostic tool for JIA. We have aimed to highlight the disease relevant information contained in the measurements, given that we do not know whether absolute parameter measurements can be directly compared between children.

In conclusion, we have found that any of the pharmacokinetic models investigated can be used to model the TMJ vascularity. A temporal resolution of at least 4 s should be used in the measurement of the DCE-MRI data. A high temporal resolution in DCE-MRI data from the TMJ holds information which is not available in corresponding lower sampled data. Elastic image registration allows motion affected data to be sufficiently recovered to be included for pharmacokinetic modelling. Motion correction thus facilitates the data analysis for evaluation of DCE-MRI as a diagnostic tool for JIA affected TMJ. To further assess the diagnostic value of high temporal resolution DCE-MRI data, as well as of motion corrected DCE-MRI data, the estimated perfusion parameters should be correlated to other clinical information in a larger study cohort.

Funding

This work was supported by the Trond Mohn Foundation [grant numbers BFS2016TMT01]; the European Regional Development Fund-Project “Modernization and support of research activities of the national infrastructure for biological and medical imaging Czech-BioImaging”

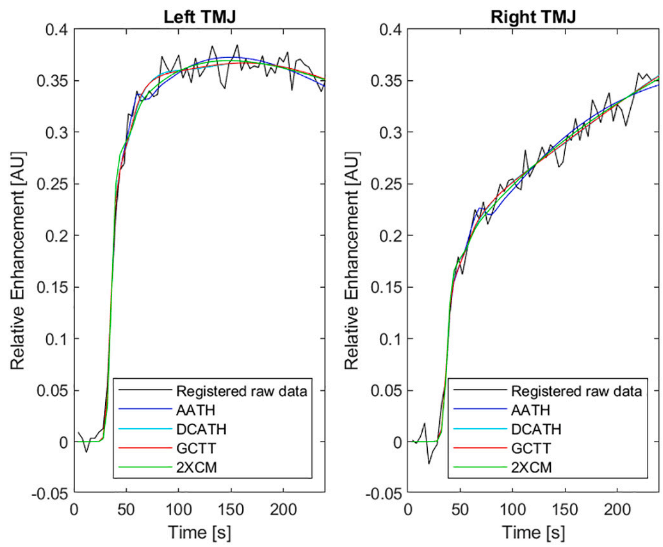

Fig. 5. A comparison of four pharmacokinetic models (Blue: Adiabatic Approximation to the Tissue Homogeneity Model (AATH), Cyan: Distributed Capillary Adiabatic Tissue Homogeneity Model (DCATH), Red: Gamma Capillary Transit Time Model (GCTT) and Green: Two Compartment Exchange Model (2CXM)) applied in a random participant. Left Temporomandibular Joint (TMJ) (left column), right TMJ (right column). Elastic motion corrected relative enhancement curves (black) are overlaid parametric model curves. (For interpretation of the references to colour in this figure legend, the reader is referred to the web version of this article.)

Table 5
Sensitivities and specificities of k-means clusters after principal component analysis. Principal component analysis was performed including all parameters defined in Table 1. The quantitative model parameters were estimated with the Adiabatic Approximation to Tissue Homogeneity (AATH) model, Distributed Capillary Adiabatic Tissue Homogeneity (DCATH) model, Gamma Capillary Transit Time (GCTT) model as well as the Two-Compartment Exchange Model (2CXM). Numbers in parentheses refer to the sensitivity and specificity of random forest machine learning predictions on the 25% of the data that was used for testing.

	AATH	DCATH	GCTT	2CXM
Sensitivity	0 (0)	0.27 (0)	0 (0)	0.18 (0)
Specificity	0.93 (0.85)	0.93 (0.85)	0.90 (0.83)	0.93 (0.85)

[grant numbers CZ.02.1.01/0.0/0.0/16_013/0001775]; the MEYS CR [grant numbers LO1212]; the Northern Norway Regional Health Authority [grant numbers; SPF1229-15]; and the Tromsø Research Foundation.

Declaration of Competing Interest

The authors have no financial interests to declare.

References

[1] Petty RE, Southwood TR, Manners P, Baum J, Glass DN, Goldenberg J, et al. International league of associations for rheumatology classification of juvenile idiopathic arthritis: second revision. J Rheumatol 2004;31:390–1.

[2] Manners PJ, Bower C. Worldwide prevalence of juvenile arthritis - why does it vary so much? J Rheumatol 2002;29:1520–30.

[3] Selvaag AM, Aulie HA, Lilleby V, Flatø B. Disease progression into adulthood and predictors of long-term active disease in juvenile idiopathic arthritis. Ann Rheum Dis 2016;75:190–5.

[4] Oliveira-Ramos F, Eusébio M, Martins FM, Mourão AF, Furtado C, Campanilho-Marques R, et al. Juvenile idiopathic arthritis in adulthood: fulfilment of classification criteria for adult rheumatic diseases, long-term outcomes and predictors of inactive disease, functional status and damage. RMD Open 2016;2. https://doi.org/10.1136/rmdopen-2016-000304.

[5] Weiss PF, Arabshahi B, Johnson A, Blaniuk LT, Zarnow D, Cahill AM, et al. High prevalence of temporomandibular joint arthritis at disease onset in children with juvenile idiopathic arthritis, as detected by magnetic resonance imaging but not by ultrasound. Arthritis Rheumatol 2008;58:1189–96.

[6] Niibo P, Pruunsild C, Voog-Oras Ü, Nikopensius T, Jagomägi T, Saag M. Contemporary management of TMJ involvement in JIA patients and its orofacial consequences. EPMA J 2016;7. https://doi.org/10.1186/s13167-016-0061-7.

[7] Twilt M, Mobers SMLM, Arends LR, ten Cate R, van Suijlekom-Smit L. Temporomandibular involvement in juvenile idiopathic arthritis. J Rheumatol 2004;31:1418–22.

[8] Küseler A, Pedersen TK, Herlin T, Gelineck J. Contrast enhanced magnetic resonance imaging as a method to diagnose early inflammatory changes in the temporomandibular joint in children with juvenile chronic arthritis. J Radiol 1998; 25:1406–12.

[9] Hauser RA, Schroeder S, Cannizzaro E, Muller L, Kellenberger CJ, Saurenmann RK. How important is early magnetic resonance imaging of the temporomandibular joint for the treatment of children with juvenile idiopathic arthritis: a retrospective analysis. Pediatric Rheumatol 2014;12. https://doi.org/10.1186/1546-0096-12-36.

[10] Karhullahti T, Ylijoki H, Rönning O. Mandibular condyle lesions related to age at onset and subtypes of juvenile rheumatoid arthritis in 15-year-old children. Scand J Dent Res 1993;101:332–8.

[11] Müller L, Kellenberger CJ, Cannizzaro E, Ettlin D, Schraner T, Bolt IB, et al. Early diagnosis of temporomandibular joint involvement in juvenile idiopathic arthritis: a pilot study comparing clinical examination and ultrasound to magnetic resonance imaging. Rheumatology 2009;48:680–5.

[12] Jank S, Haase S, Strobl H, Michels H, Häfner R, Missmann N, et al. Sonographic investigation of the temporomandibular joint in patients with juvenile idiopathic arthritis: a pilot study. Arthritis Rheum 2007;57:213–8.

[13] Ronchezel MV, Hilário MO, Goldenberg J, Ledermann HM, Faltin KJ, Azevedo MF, et al. Temporomandibular joint and mandibular growth alterations in patients with juvenile rheumatoid arthritis. J Rheumatol 1995;22:1956–61.

[14] Suenaga S, Hamamoto S, Kawano K, Higashida Y, Noikura T, Dynamic MR. Imaging of the temporomandibular joint in patients with arthrosis: relationship

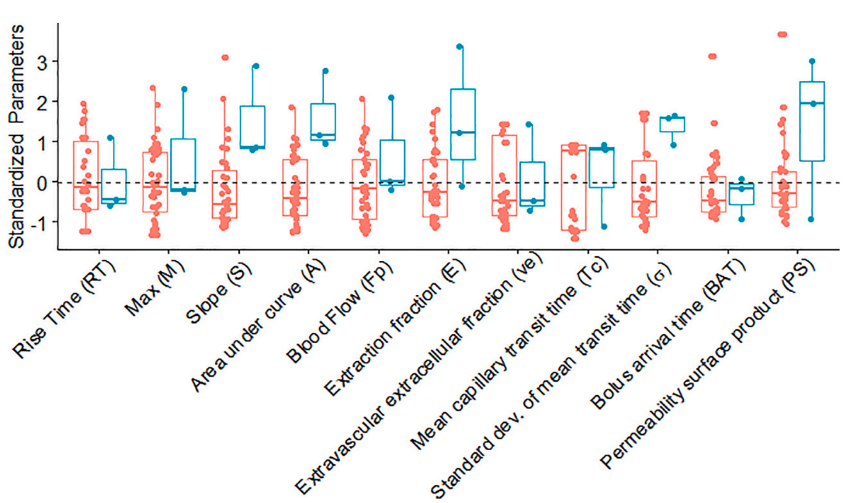

Fig. 6. Standardized relative parameter differences calculated using the Distributed Capillary Adiabatic Tissue Homogeneity (DCATH) model and semi-quantitative parameters in the assumed unaffected participants (Group A; red) and assumed affected participants (Group B; blue) in the 41 cases where there is agreement on diagnosis between the k-means clustering and structural image scores. (For interpretation of the references to colour in this figure legend, the reader is referred to the web version of this article.)

between contrast enhancement of the posterior disk attachment and joint pain. AJR Am 1996;166:1475–81.
[15] Tasali N, Cubuk R, Aricak M, Ozarar M, Saydam B, Nur H, et al. Temporomandibular joint (TMJ) pain revisited with dynamic contrast-enhanced magnetic resonance imaging (DCE-MRI). Eur J Radiol 2011;81:603–8.
[16] Xiong X, Ye Z, Tang H, Wei Y, Nie L, Wei X, et al. MRI of temporomandibular joint disorders: recent advances and future directions. J Magn Reson Imaging 2020;0. https://doi.org/10.1002/jmri.27338.
[17] Sano T, Westesson P-L. Magnetic resonance imaging of the temporomandibular joint: increased T2 signal in the retrodiskal tissue of painful joints. Oral Surg Oral Med Oral Pathol Oral Radiol Endod 1995;79:511–6.
[18] Rosen BR, Belliveau JW, Vevea JM, Brady TJ. Perfusion imaging with NMR contrast agents. Magn Reson Med 1990;14:249–65.
[19] Chen W, Giger ML, Bick U, Newstead GM. Automatic identification and classification of characteristic kinetic curves of breast lesions on DCE-MRI. Med Phys 2006;33:2878–87.
[20] Schabel MC. A unified impulse response model for DCE-MRI. Magn Reson Med 2012;68:1632–46.
[21] Sourbron SP, Buckley DL. Tracer kinetic modelling in MRI: estimating perfusion and capillary permeability. Phys Med Biol 2011;57:R1–33.
[22] Sourbron SP, Buckley DL. Classic models for dynamic contrast-enhanced MRI. NMR Biomed 2013;26:1004–27.
[23] Starck LS, Andersen E, Macíček O, Jiřík R, Angenete O, Augdal T, et al. Effects of image registration in dynamic contrast enhanced MRI of the TMJ. In: Proceedings of the 27th Annual Meeting of ISMRM, Montréal; 2019 (abstract 4490).
[24] Parker GJ, Roberts C, Macdonald A, Buonaccorsi GA, Cheung S, Buckley DL, et al. Experimentally-derived functional form for a population-averaged high-temporal-resolution arterial input function for dynamic contrast-enhanced MRI. Magn Reson Med 2006;56:993–1000.
[25] Macíček O, Jiřík R, Mikulka J, Bartoš M, Šprláková-Puková A, Keřkovský M, et al. Time-efficient perfusion imaging using DCE- and DSC-MRI. Measure Sci Rev 2018;18:262–71.
[26] Demant S, Hermann NV, Darvann TA, Zak M, Schatz H, Larsen P, et al. 3D analysis of facial asymmetry in subjects with juvenile idiopathic arthritis. Rheumatology 2011;50:586–92.
[27] St. Lawrence KS, Lee T-Y. An adiabatic approximation to the tissue homogeneity model for water exchange in the brain: I. theoretical derivation. J Cereb Blood Flow Metab 1998;18:1365–77.
[28] St. Lawrence KS, Lee T-Y. An adiabatic approximation to the tissue homogeneity model for water exchange in the brain: II. Experimental validation. J Cereb Blood Flow Metab 1998;18:1378–85.
[29] Bartoš M, Jiřík R, Kratochvíla J, Standara M, Starčuk Z, Taxt T. The precision of DCE-MRI using the tissue homogeneity model with continuous formulation of the perfusion parameters. Magn Reson Imaging 2014;32:505–13.
[30] Koh TS, Zeman V, Darko J, Lee T-Y, Milosevic MF, Haide M, et al. The inclusion of capillary distribution in the adiabatic tissue homogeneity model of blood flow. Phys Med Biol 2001;46:1519–838.
[31] Klein S, Staring M, Murphy K, Viergever MA, JPW Pluim. Elastix: a toolbox for intensity based medical image registration. IEEE Trans Med Imaging 2010;29:196–205.
[32] Shamonin DP, Bron EE, Lelieveldt BPF, Klein MSS, Staring M. Fast parallel image registration on CPU and GPU for diagnostic classification of Alzheimer's disease. Front Neuroinform 2014;7:1–15.
[33] Van't Klooster R, Staring M, Klein S. Automated registration of multispectral MR vessel wall images of the carotid artery. Med Phys 2014;40. https://doi.org/10.1118/1.4829503.
[34] van't Klooster R. Open Source Image Registration Parameter File. 2020. "http://elastix.bigr.nl/wiki/index.php/Parameter_file_database," 3 March 2020. [Online]. Available: http://elastix.bigr.nl/wiki/images/8/89/Par0018_3D_affine_MI.txt . [Accessed 2020 May 21].
[35] Maes F, Collignon A, Vandermeulen D, Marchal G, Suetens P. Multimodality image registration by maximization of mutual information. IEEE Trans Med Imaging 2006;16:187–98.
[36] Klein S, Pluim JPW, Staring M, Viergever MA. Adaptive stochastic gradient descent optimisation for image registration. Int J Comput Vis 2009;81:227–39.
[37] Hodneland E, Lundervold A, Rørvik J, Munthe-Kaas AZ. Normalized gradient fields for nonlinear motion correction of DCE-MRI time series. Comput Med Imaging Graph 2014;38:202–10.
[38] Pedregosa F, Varoquaux G, Gramfort A, Michel V, Thirion B, Grisel O, et al. Machine learning with python. J Mach Learn Res 2011;12(85):2825–30.
[39] Koopman T, Martens RM, Lavini C, Yaqub M, Castelijns JA, Boellaard R, et al. Repeatability of arterial input functions and kinetic parameters in muscle obtained by dynamic contrast enhanced MR imaging of the head and neck. Magn Reson Imaging 2020;68:1–8.